"Plug and play" full-dimensional *ab initio* potential energy and dipole moment surfaces and anharmonic vibrational analysis for CH_4-H_2O.

Chen Qu,[a] Riccardo Conte, [a] Paul L. Houston[b,c] and Joel M. Bowman [a*]

Received Xth XXXXXXXXXX 20XX, Accepted Xth XXXXXXXXX 20XX
First published on the web Xth XXXXXXXXXX 20XX
DOI: 10.1039/b000000x

The potential energy surface of the methane-water dimer is represented as the sum of a new intrinsic two-body potential energy surface and pre-existing intramolecular potentials for the monomers. Different fits of the CH_4-H_2O intrinsic two-body energy are reported. All these fits are based on 30,467 *ab initio* interaction energies computed at CCSD(T)-F12b/haTZ (aug-cc-pVTZ for C and O, cc-pVTZ for H) level of theory. The benchmark fit is a full-dimensional, permutationally-invariant analytical representation with root-mean-square (rms) fitting error of 3.5 cm^{-1}. Two other computationally more efficient two-body potentials are also reported, albeit with larger rms fitting errors. Of these a compact permutationally invariant fit is shown to be the best one in combining precision and speed of evaluation. An intrinsic two-body dipole moment surface is also obtained, based on MP2/haTZ expectation values, with an rms fitting error of 0.002 au. As with the potential, this dipole moment surface is combined with existing monomer ones to obtain the full surface. The vibrational ground state of the dimer and dissociation energy, D_0, are determined by Diffusion Monte Carlo calculations, and MULTIMODE calculations are performed for the IR spectrum of the intramolecular modes. The relative accuracy of the different intrinsic two-body potentials is analyzed by comparing the energetics and the harmonic frequencies of the global minimum well, and the maximum impact parameter employed in a sample methane-water scattering calculation.

1 Introduction

The interaction between methane and water is essential for the study of methane-water clathrates, and to understand hydrophobic interactions. It also plays an important role in combustion chemistry and related gas-phase scattering investigations. Methane clathrates have attracted extensive interest because they are a potential source of energy,[1] and their formation in gas pipelines may be responsible for flow reduction. The formation and dissociation of the clathrates have been recently studied by means of molecular dynamics (see, for instance, Ref. 2–7). At the same time, methane-water still represents a widely used model system for the study of hydrophobic interactions.[8–10] In combustion chemistry, energy transfer and dissociation of methane CH_4 (+M) $\rightleftharpoons$ CH_3+H (+M) is of interest, with particular focus on the collisional efficiency of M=H_2O.[11,12] The CH_4-H_2O collisional system has been recently investigated by means of direct-dynamics[12] to obtain moments of the energy transfer, that can be well-converged by means of only a few hundred trajectories. This has contributed to validate some energy transfer models and to compare the efficiencies of different collision partners with methane.[13,14] However, finer collisional energy transfer details, such as rare, but highly efficient energy-transfer events, detailed vibration-vibration energy transfer, etc. need a much larger number of trajectories, that are not feasible to do by means of direct dynamics. These can be obtained with fitted potential energy surfaces (PESs). Model analytical potentials have been used to perform quasi-classical trajectory (QCT) simulations of the collisional energy transfer for several systems (see, for instance, Refs. 15–17), but a realistic full-dimensional potential for CH_4-H_2O is necessary to obtain high accuracy.

The methane-water interaction has been examined with various *ab initio* methods, and several analytical forms of the PES for rigid monomers have been presented. The earliest studies (for example see Ref. 18–21) either fail to correctly identify the minimum structure or do not explore the full configuration space, due to low-level *ab initio* methods. Szczęśniak *et al.*[22] and Rovira *et al.*[23] successfully identified two minima in the PES, but the electronic binding energy of the global minimum was underestimated. The latter also reported the harmonic vibrational frequencies of the dimer. Two six-dimensional PESs for rigid monomers have been reported.[24,25] In the more recent work of Akin-Ojo and Szalewicz[25] the electronic binding energy was given as 361 cm^{-1} by extrapolating CCSD(T)/aug-cc-pVQZ and aug-cc-

[a] *Department of Chemistry and Cherry L. Emerson Centrer for Scientific Computations, Emory University, Atlanta, GA 30322, USA. E-mail: jmbowma@emory.edu*
[b] *School of Chemistry and Biochemistry, Georgia Institute of Technology, Atlanta, GA 30332, USA*
[c] *Department of Chemistry and Chemical Biology, Cornell University, Ithaca, NY 14852, USA*

pV5Z results to the complete basis set (CBS) limit. More recently, Copeland and Tschumper[26] characterized the energetics of the dimer PES with high-level CCSD(T)-F12b/VTZ-F12 calculations, and reported the binding energy of 339 cm^{-1} with counterpoise (CP) correction and 353 cm^{-1} without the correction for the global minimum; these authors also reported the binding energy of 224 and 231 cm^{-1} with and without CP correction for the higher energy minimum. However, none of the analytical PESs mentioned[20–22,24,25] is full-dimensional and so cannot be used to investigate observables that depend on the monomer vibrational motion. We report such PESs here. In addition, we present a dipole moment surface; this has not been reported previously.

Considering our future applications of this potential to energy transfer studies and properties of $CH_4(H_2O)_n$ clusters, for example methane clathrates, we employ the many-body representation for the methane-water dimer, i.e., representing the full PES as the sum of flexible monomer PESs plus an intrinsic two-body interaction. The focus here is on the latter, in full dimensionality. Specifically, we obtain a new PES for the intrinsic two-body energy, which is defined as

$$V_{2b} = V_{dimer} - V_{CH_4} - V_{H_2O}, \quad (1)$$

where the potentials for the isolated monomers are given using obvious notation. In principle, the dimer and intrinsic two-body potentials should be invariant with respect to all permutations of like atoms. However, for the non-covalent interaction relevant here, it is not necessary to consider the permutations of H atoms of H_2O with those of CH_4.

A suitable approach to represent this symmetry in a fitting basis comes from the theory of invariant polynomials. A computationally efficient implementation of this approach consists in defining a set of primary and secondary invariants,[27] while a second one is based on monomial symmetrization.[28] Both methods can provide essentially equivalent, very precise fits to a data set of electronic energies. However, while much faster to evaluate than even low-level direct dynamics calculations, these representations are generally significantly slower to evaluate than commonly used model potentials. In applications involving methane clathrates, we need to evaluate the intrinsic potential for each CH_4-H_2O pair, so the computational cost can be high. Three of us have recently introduced a compact fitting procedure[29,30] that removes polynomials depending on the intramolecular distances in the monomial symmetrization approach, and guarantees zero intrinsic two-body energy at the dissociation limit. This procedure significantly speeds up the potential evaluation, but at the cost of lower fitting precision. A different family of fitting techniques is represented by sum-of-pairs methods, based on a limited number of non-linear parameters.[31] Sum-of-pairs methods have the advantages that they require only a limited number of *ab initio* energies for the fit and that qualitatively correct physical behavior is ensured in all configurational regions, even where *ab initio* energies have not been calculated. However, pairwise fits may be not very accurate or appropriate to describe systems (like methane-water) where orientation dependence is expected to influence significantly the interaction. Furthermore, they are based on two-body atomic interactions, thus missing multi-atom contributions which are relevant at short distances, a region of key importance for energy transfer.

In this article, we present a full-dimensional, permutationally invariant fit to the methane-water intrinsic two-body potential, based on the primary and secondary invariants approach. Other compact and sum-of-pairs fits are also reported. By adding existing monomer potentials of CH_4 and H_2O, a full PES of the CH_4-H_2O dimer is obtained. There are numerous choices for these monomer potentials and specific ones will be dictated by the planned usage of the PES. We discuss this further in Section 2. A dipole moment surface (DMS) is presented as well. The different intrinsic two-body PESs are compared in terms of the root-mean-square (rms) fitting error, the speed of potential evaluation, the energetics, the harmonic frequencies as well as the maximum impact parameter for bimolecular scattering simulations. Diffusion Monte Carlo (DMC) and MULTIMODE calculations are performed to characterize the zero-point properties and intramolecular vibrational fundamentals and IR spectrum of the dimer.

The paper is organized as follows. In Section 2, we provide the theoretical and computational details of the *ab initio* calculation, the fitting methods, the DMC and MULTIMODE calculations. In Section 3, we report the results of the comparisons of the two-body PESs, the vibrational analysis, the IR spectra, and collision dynamics. The conclusions and final remarks are given in Section 4.

2 Theoretical and Computational Details

2.1 *Ab initio* calculations

The database of 30,467 configurations and energies was obtained as follows. Seven C-O distances were picked in the range from 3.0 to 10.0 Å, and at each distance, 3,200 monomer geometries were chosen with different orientations. 4,932 additional configurations of the dimer were generated using *ab initio* molecular dynamics at the DFT (B3LYP) level of theory. An initial fit then was performed based on the 27,332 points described above. The remaining 3,135 points were calculated to provide better coverage of the initial PES, based primarily on running DMC calculations of the dimer zero-point energy and also to improve the harmonic frequencies at the two minima.

The CCSD(T)-F12b method[32,33] with haTZ (aug-cc-pVTZ for C and O, and cc-pVTZ for H) basis set was employed to calculate the energies, using MOLPRO 2010.[34] For each

dimer configuration, the energies of the dimer and the isolated monomers at that configuration were calculated, and the intrinsic two-body energy was obtained according to equation (1) without counter-poise (CP) correction. (See Section 3.1 for more discussion of the CP correction.) Overall, the computational cost of calculating the 30,467 points in the database can be converted to roughly 13 days of CPU time on a 16-processor computer.

The expectation value of the three dipole moment components of the dimer were calculated at MP2 level of theory with haTZ basis set, also using MOLPRO 2010. The dipole moments of the isolated monomers were also calculated at the same level of theory in order to obtain the intrinsic two-body dipole given by:

$$\vec{\mu}_{2b} = \vec{\mu}_{dimer} - \vec{\mu}_{CH_4} - \vec{\mu}_{H_2O}. \qquad (2)$$

CCSD(T)-F12b/haTZ level of theory is both high and computationally feasible for the large data set of electronic energies. For the dipole moments, MP2 provides a reasonable, if not "high-resolution" level of theory that is computationally efficient.

2.2 PES and DMS fitting

Three least-squares fits of the 30,467 intrinsic two-body energies were performed. For the two polynomial fits, the maximum polynomial order was set to five, and the permutation group is appropriate for A_4B_2CD. As noted above, this means that hydrogen atoms belonging to different monomers do not permute, so the PES is not invariant to intermolecular hydrogen exchange, which is not feasible for the interactions of interest. Thus, the permutation order is 4!2! = 48. The polynomial variables are Morse exponentials $y_{ij} = \exp(-r_{ij}/\alpha)$, where α is a parameter usually between 2.0 and 3.0 au (α = 2.0 au for these PESs), and r_{ij} is the internuclear distance between atom i and j. The choice of Morse exponentials as variables instead of the simpler internuclear distances allows the fitted PESs to describe dissociation without divergence.

The best fitted intrinsic two-body potential, denoted by PES_{2b}-PI, is based on a rigorous decomposition into primary and secondary invariant polynomials,[27] leading to a total of 10,220 linear coefficients. PES_{2b}-PI provides the benchmark for our calculations.

A second fitted two-body potential, denoted PES_{2b}-CSM, is a compact one using symmetrized monomials, where by "compact" we mean that the fit depends explicitly only on intermolecular distances.[30] The starting point to build PES_{2b}-CSM is the full (F) expansion of the intrinsic potential in terms of symmetrized monomials,[27]

$$V_{2b}^{F} = \sum_{m=0}^{M} D_{\underline{b}} \mathscr{S} \left[\prod_{i<j}^{N} y_{ij}^{b_{ij}} \right] \qquad (m = \sum b_{ij}), \qquad (3)$$

where M is the maximum polynomial order, $D_{\underline{b}}$ are the linear coefficients and $\underline{b}$ stands for the ordered collection of the exponents b_{ij}; $\mathscr{S}$ is the formal operator that symmetrizes monomials, and N is the number of atoms in the system. A computationally-efficient factorization scheme to obtain these polynomials iteratively has been reported.[28] The scheme is not as efficient as the invariant polynomial factorization. However, it is more straightforward to modify this scheme to create PES_{2b}-CSM, as we describe next.

To extract the desired subset of polynomials for PES_{2b}-CSM of the methane-water system, the 28 Morse variables are defined as shown in Fig. 1. The circled variables correspond to the thirteen intramolecular Morse variables (ten for methane plus three for water), and they are set equal to zero. Instead, a different non-zero value is assigned to each one of the remaining fifteen intermolecular Morse variables. By calculating monomial values after these substitutions, all monomials with intramolecular dependence return a null value and can be eliminated from the monomial list used for PES_{2b}-CSM. The ensuing elimination of some polynomials from the full representation in equation (3) can result in a substantial compaction of the number of terms in that representation.

This compact two-body PES results in a substantial speed-up in the potential evaluation. For this intrinsic two-body methane-water potential, PES_{2b}-CSM contains only 841 linear coefficient (and thus polynomial evaluations), compared to the 10,220 needed by PES_{2b}-PI. Furthermore, PES_{2b}-CSM fixes by construction the issue of small non-zero intrinsic two-body energy at large distances, that can occur in PES_{2b}-PI due to lack of rigorous separation of some terms in that representation.[27]

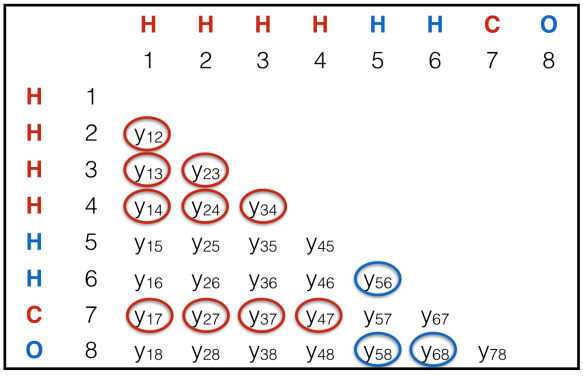

Fig. 1 Table of Morse variables for the CH_4-H_2O system. Red circles indicate the ten Morse variables dependent on methane intramolecular distances, while the blue circles show the three water intramolecular Morse variables.

The third fitted two-body potential, denoted PES_{2b}-P24, is a pairwise one based on 24 non-linear parameters, six for each pair of intermolecular atomic species (C-O; C-H_W; H_M-O;

H_M-H_W. H_W indicates a water hydrogen, while H_M a hydrogen of the methane molecule). The mathematical expression for this sum-of-pairs fit is the one proposed by Varandas and Rodrigues [31] and it has been successfully applied to a number of systems (see, for instance, refs. 35–37). The potential is expressed as a sum-of-pairs contribution dependent on distances between the four intermolecular couples of atoms in the CH_4-H_2O system (see equations (4)–(5)).

$$V_{2b}^{\mathrm{P24}} = \sum_{i,j} V(r_{ij}) \qquad i,j = \mathrm{C}, \mathrm{H_M}, \mathrm{H_W}, \mathrm{O} \tag{4}$$

$$V(r_{ij}) = A_{ij}\, exp(-b_{ij} r_{ij}) - \sum_n \chi_n(r_{ij}; R_{0,ij}) \frac{C_{n,ij}}{r_{ij}^n} \quad n = 6,8,10 \tag{5}$$

The damping χ functions in equation (5) are defined explicitly in equations (8)-(11) of Ref. 31. The parameters were obtained using a standard least-squares procedure.

The intrinsic two-body dipole moment is represented in the form

$$\vec{\mu}_{2b}(R) = \sum_i w_i(R) \vec{r}_i, \tag{6}$$

where R denotes the nuclear configuration and $\vec{r}_i$ is the set of Cartesian coordinates of the ith nucleus. $w_i(R)$ is the effective charge on the ith nucleus, which is a scalar quantity that can be expanded by polynomials of the Morse variables. The dipole moment should also be invariant under permutations of like atoms, so the property of the effective charge $w_i(R)$ under permutations of identical atoms is different from that of the potential, described as follows. For example, if we exchange identical nuclei i and j, the configuration transforms from R to R', and the effective charge on these two nuclei must satisfy

$$(w_j(R'), w_i(R')) = (w_i(R), w_j(R)). \tag{7}$$

The effective charges on *other* atoms must be invariant to this permutation. The details of the DMS fitting can be found in Ref. 38.

Finally, the complete PES and DMS are the sum of the intrinsic two-body terms, described above, and the methane and water monomer permutationally-invariant PESs and covariant DMSs, respectively. The methane monomer PES and DMS are taken from previous global *ab initio* ones using the invariant polynomial approach by Warmbier *et al.* [39]. This PES dissociates to fragments CH_3+H and so is suitable for use in studies of energy transfer involving highly excited methane. The water monomer PES is the Partridge-Schwenke one,[40] which is spectroscopically accurate, while for convenience the monomer dipole of H_2O is extracted from the WHBB water dipole moment.[38] The full CH_4-H_2O potentials using the three intrinsic two-body potentials are denoted, using obvious notation, PES-PI, PES-CSM and PES-P24. Note, that it is straightforward to incorporate other monomer potentials and dipole moment surfaces to improve the accuracy of the full potential of the dimer for given applications. This is the "plug and play" aspect of the approach given in the title. For example, other accurate PESs exist for methane, e.g., a recent one due to Tennyson and co-workers [41] as well as a highly accurate DMS for H_2O, also due to Tennyson and co-workers.[42] Thus, for certain applications the complete PES could be more accurate than a full PES fit to even higher-level *ab initio* electronic energies than considered here.

2.3 Diffusion Monte Carlo and MULTIMODE calculations

Standard Diffusion Monte Carlo calculations were performed to obtain the rigorous zero-point energy (ZPE) of the dimer and the fragments and to characterize the properties of the vibrational ground-state wave function. The simplest unbiased algorithm [43–45] was used in our simulations. Ten "trajectories" were performed for the bound dimer and the fragments; in each simulation, 20,000 walkers were propagated for 25,000 steps. The walkers were first equilibrated for 5,000 steps and the energies of the remaining 20,000 steps were collected to compute the reference energy.

The vibrational ground-state wave function is visualized as an isosurface. Each walker was optimally aligned into a reference frame. The space was divided into volume elements and a statistical analysis was performed for each volume element to obtain the wave function amplitude in that volume.

Single-reference MULTIMODE [46] calculations were done to calculate the vibrational eigenstates for the high-frequency intramolecular modes with J=0. Two approaches were taken. In the first, we performed a standard normal-mode analysis for the bound dimer and selected the twelve intramolecular modes in subsequent vibrational self-consistent field/Vibrational configuration interaction (VSCF/VCI) calculations. Specifically, a twelve-dimensional Schrödinger equation

$$\hat{H}(\mathbf{Q})\Psi(\mathbf{Q}) = E\Psi(\mathbf{Q}) \tag{8}$$

was solved. $\mathbf{Q} = [Q_1\ Q_2\ \cdots\ Q_{12}]$ denotes the twelve intramolecular modes. The remaining intermolecular modes were fixed at their values (zero) at the global minimum. The potential term in the Hamiltonian was represented by a hierarchical n-mode representation; in this twelve-mode calculation, it was truncated at 4-mode representation. The representation is adequate to produce well-converged results, as demonstrated for methane.[47] We employed seven harmonic-oscillator wave functions for each mode as basis to expand the VSCF states. The VSCF ground and virtual states were then used to expand the CI states in the virtual state CI calculation (VCI). In the VCI calculation, simultaneous excitation of up to four modes were done; the maximum excitation of a single

mode was seven, six, five and four respectively in one-, two-, three- and four-mode basis, and the sum of quanta of excitation was seven. In addition, we exploited the C_s symmetry of the dimer, which allowed to separate the Hamiltonian matrix into two symmetry blocks of sizes 15,374 and 11,122. This same approach has been successfully applied to calculate the intramolecular frequencies and IR spectra of H_7^+ and D_7^+.[48]

The second approach is the local monomer method (LMon).[49] In LMon, a normal-mode analysis and VSCF/VCI are applied to each monomer but using the full potential. This approach has been adopted in various systems including water clusters,[49,50] ice,[51,52] and HCl clusters.[53] This strategy results in a substantial reduction in the computational effort. In the present case, methane has nine high-frequencies modes and water has only three. Therefore, in LMon calculations one nine-mode and one three-mode calculation are done, instead of a larger twelve-mode calculation. Thus, if the same number of basis functions and the same restrictions for excitation of a single mode and sum of quanta had been imposed, the size of the two symmetry blocks for methane would only have been 4,350 and 3,820. In practice, we were able to increase the number of basis functions and the maximum excitation for a single mode to nine without dealing with a bigger CI matrix. Four-mode representation of the potential was applied in the LMon calculation of methane, and the sizes of the two symmetry blocks were 12,995 and 11,315. Three-mode representation was applied for water monomer, as it has only three intramolecular modes. The maximum excitation of a single mode was set to ten, and the sum of quanta of excitation was restricted to be ten, fifteen and twenty in one-, two- and three-mode basis. The VCI matrix size was only 1,066 even without exploiting symmetry. It is important to assess the accuracy of this approach for the dimer as it is the only feasible one for larger complexes such as methane clathrates.

Intensities of vibrational transitions were calculated using the "dump-restart" procedure in MULTIMODE, as described in Ref. 54. In brief, the wave functions of different vibrational eigenstates were extracted and the transition elements calculated according to

$$R_{\alpha if} = \int \Psi_i(\mathbf{Q})\mu_\alpha(\mathbf{Q})\Psi_f(\mathbf{Q})d\mathbf{Q}, \qquad (9)$$

where $\mathbf{Q}$ is the set of normal coordinates and $\mu_\alpha(\mathbf{Q})$ is the α component ($\alpha = x,\ y,\ z$) of the dipole moment. Ψ_i and Ψ_f are the initial and final state of the transition. The intensity is proportional to the wavenumber (ν) of the transition multiplied by the square of the 2-norm of the three transition element vector $[R_{xif}\ R_{yif}\ R_{zif}]$:

$$I_{if} \propto \nu \sum_\alpha \left|R_{\alpha if}\right|^2. \qquad (10)$$

3 Results and Discussion

3.1 Fitting accuracy and binding energy

The energy distribution of the 30,467 points and the cumulative rms error of PES_{2b}-PI are shown in Fig. 2. Many points were sampled in the attractive region to ensure a good description near the potential minima. In addition, more than 10,000 energies are in the range from -50 to 50 cm^{-1}. Most of the corresponding geometries have a large C-O distance, so the interaction is very weak. This set of points forces PES_{2b}-PI towards the correct zero value of the intrinsic two-body energy at large monomer separation.

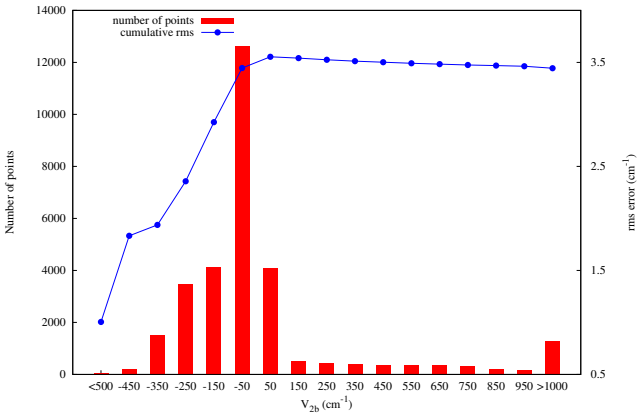

Fig. 2 Energy distribution of the 30,467 points and cumulative rms error of PES_{2b}-PI.

Table 1 Parameters for the pairwise fitted two-body potential (PES_{2b}-P24)

	C-O	C-H_W	H_M-O	H_M-H_W
C_6	1.1875	2.3968	0.7648	8.6842
C_8	0.9954	0.8829	0.8904	0.9811
C_{10}	0.9996	0.9879	0.9893	0.9799
A	1.3898	15.5380	5.1553	5.3966
b	1.3135	2.3858	1.8655	1.9730
R_0	1.0022	1.6074	1.4605	0.4248

The parameters of PES_{2b}-P24 were determined by nonlinear least squares minimization, as usual, and are given in Table 1. The computational efficiency of the three two-body potentials was determined by calculating the time needed for 50,000 potential calls averaged over batches of ten repetitions. Table 2 reports the number of coefficients, energy-dependent rms errors, and computational times for the three two-body potentials. PES_{2b}-PI, as expected, is the most accurate one. PES_{2b}-CSM removes all the terms containing intramolecular distances, so the number of coefficients is decreased by an order of magnitude. The effect is that potential calls are much

faster, and only 8% of the time for PES_{2b}-PI is necessary. PES_{2b}-CSM is globally less accurate with a higher rms fitting error but as seen below still quite accurate. Finally, PES_{2b}-P24 is characterized by an even larger rms error, while the very reduced number of coefficients yields only a partial reduction of computational costs. The reason is that the mathematical expressions to evaluate in the case of PES_{2b}-P24 (Equation (4)–(5)) are much more computationally expensive than the Morse variables.

Table 2 Number of coefficients, rms fitting error for different energy regions (cm^{-1}), and computational times (arbitrary units) for the three two-body PESs. The computational time for PES_{2b}-PI is arbitrarily set equal to 100 to facilitate the comparison

	PES_{2b}-PI	PES_{2b}-CSM	PES_{2b}-P24
N. coeff.	10,220	841	24
rms (E<0)	3.4	39.8	135.4
rms (0<E<1,500)	3.5	95.0	265.2
rms (E>1,500)	3.5	162.6	643.1
rms (total)	3.5	64.1	204.1
t	100.0	8.0	5.6

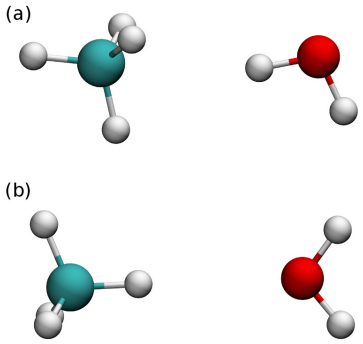

Fig. 3 Structures of the two stationary points on the PES: (a) global minimum; (b) secondary minimum.

Two minima are located on the PESs. Both PES-PI and PES-CSM reproduce the correct geometries indicated in Fig. 3. In the lower energy one the water monomer is a hydrogen bond donor, while it becomes an acceptor in the higher-energy minimum. Both of the two minima have C_s symmetry. Selected bond lengths and bond angles of the two minima are listed in Table 3, from direct *ab initio* optimization and the PES-PI. The optimized geometries from PES-PI agree very well with the CCSD(T)-F12b/haTZ ones, which is expected due to the small fitting error. In addition, our geometries agree well with previous calculations, as shown in the table. The energies of the minima on the PESs as well as the *ab initio* results with and without CP correction are listed in Table 4. The CP correction for the global and secondary minima is about 20 cm^{-1}, which is not large. The binding energy of the global minimum without CP correction agree very well with the CCSD(T)/CBS result,[25] presumably by cancellation of errors due to basis set superposition and basis incompleteness. Because of the fortuitously close agreement with the benchmark, the PES was fit to electronic energies without the CP correction. Our binding energy for the secondary minimum is slightly larger than the value reported by Copeland and Tschumper[26]. The agreement between the different PESs is good, apart from PES-P24, which is not able to accurately give the energies of the two minima. It also predicts a somewhat different equilibrium geometry.

Table 3 Bond lengths (in Å) and angles (in degree) of the two minima

	ab initio [a]	PES-PI	Ref. 25
Global min. $r_{C\text{-}O}$	3.470	3.472	3.51 [b], 3.49 [c]
O–H···C angle	167.6	168.0	165.6 [b], 165.3 [c]
Secondary min. $r_{C\text{-}O}$	3.707	3.705	3.76 [b], 3.71 [c]

[a] CCSD(T)-F12b/haTZ. [b] CCSD(T). [c] SAPT.

Table 4 Interaction energies (cm^{-1}) of the global and secondary minima

	Global	Secondary
ab initio with CP	330	223
ab initio without CP	356	243
PES-PI	357	243
PES-CSM	366	243
PES-P24	279	20

In Fig. 4 we show two unrelaxed one-dimensional cuts as a function of the C-O distance and calculated with PES_{2b}-PI and PES_{2b}-CSM, as well as *ab initio* energies along these cuts, at the global minimum and secondary minimum orientations. PES_{2b}-PI agrees very well with *ab initio* points, as anticipated by the small rms fitting error. Generally, PES_{2b}-CSM is also in good agreement, except between 3.5 and 5.0 Å at the global minimum orientation. The energies of both intrinsic two-body PESs go to zero when the distance becomes large, but due to different reasons. PES_{2b}-CSM is by construction zero at large C-O distances, while PES_{2b}-PI is zero because we sampled a large number of data in that region.

To go a step further from the electronic binding energy to the measurable dissociation energy, we rigorously calculated the ZPE of the bound dimer and isolated fragments using DMC. The ZPE of the dimer is 14,510±5 cm^{-1}, and the sum of the ZPEs of the isolated fragments (CH_4+H_2O) is 14,663±4 cm^{-1} relative to the global minimum. Thus, we determine the dissociation energy D_0 of the dimer is 153±11 cm^{-1}. The statistical error in the ZPE of the dimer (5 cm^{-1})

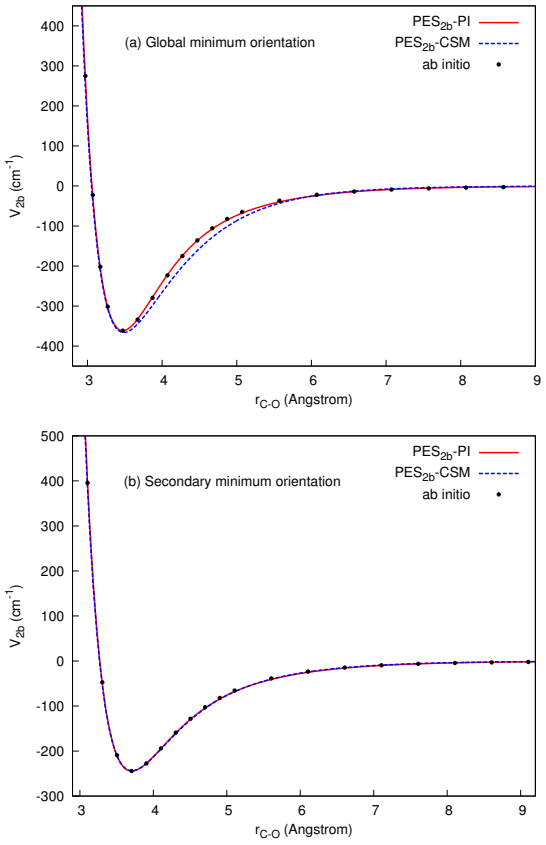

Fig. 4 Two unrelaxed one-dimensional cuts from PES_{2b}-PI, PES_{2b}-CSM and *ab initio* calculations: intrinsic two-body energy as a function of C-O distance at (a) the global minimum orientation, and at (b) the secondary minimum orientation.

and sum of ZPEs of the isolated fragments (4 cm^{-1}) leads to a statistical error of 6.4 cm^{-1} for D_0. We give a conservative estimate of the uncertainty as the sum of the statistical error (6.4 cm^{-1}) and the systematic error of our D_e compared to the CCSD(T)/CBS value (4 cm^{-1}). DMC simulations were also performed on PES-CSM, and the ZPE of the bound dimer is 14,514±6 cm^{-1}, which agrees very well with the ZPE value from PES-PI, and remarkably predicts a D_0 value (149 cm^{-1}) within the uncertainty range of PES-PI.

3.2 Vibrational analysis

The vibrational ground state wave function obtained from a DMC simulation that employs the PES-PI potential is shown in Fig. 5. As expected, the motion of heavy atoms (C and O) is more localized, than the H atom motion. When the isovalue is 50% of the maximum, the hydrogen wave function is still somewhat localized, while at 25% of the maximum amplitude, the wave function is spherical. This indicates that the

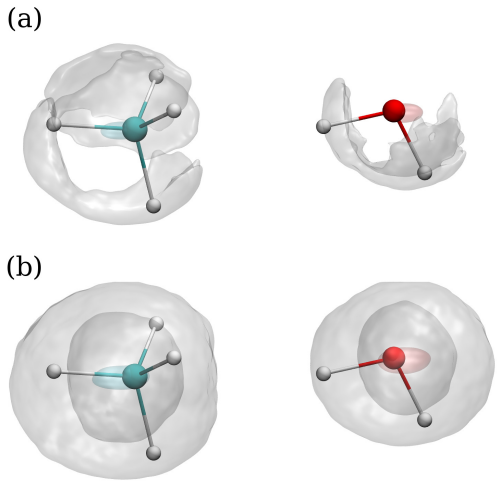

Fig. 5 Vibrational ground state wave function of CH_4-H_2O dimer. The isovalue is 50% of the maximum wave function amplitude in (a), and 25% in (b).

monomers are undergoing large-amplitude internal rotation in the bound dimer, which agrees with the conclusion of experimental findings.[55,56] The experimental microwave and far infrared spectra obtained in these experiments are reproduced reasonably well by simulations employing an internal-rotation model. In the two experiments, the authors reported a average distance of 3.70 Å bewteen CH_4 and H_2O centers of mass, R_0, based on an analysis using a model Hamiltonian. This distance lies between our global minimum (3.44 Å) and the secondary minimum (3.77 Å). Our estimate of this distance using DMC walkers is 3.78 Å. Agreement with the result from experimental modeling is good but not excellent. The weak binding of the complex and the presence of two minima with very different values R_e make a highly accurate determination of the expectation value R very difficult.

The harmonic frequencies of the complex at the global minimum from CCSD(T)-F12b/haTZ calculations, PES-PI and PES-CSM are listed in Table 5. In addition, intramolecular harmonic frequencies from the LMon calculations using PES-PI and the frequencies of the isolated monomers are given. First, as seen, the results using PES-PI and PES-CSM are in good agreement with each other and also with the direct *ab initio* results. Note, that even with a "perfect" fit of the intrinsic two-body interaction, perfect agreement with the CCSD(T)-F12b/haTZ frequencies is not expected because the monomer potentials used in the PESs are calculated at a different level of theory. The frequencies from the LMon and full normal mode analysis using PES-PI are virtually identical, indicating, as expected, that LMon is a very good approximation for this

Table 5 Harmonic frequencies (cm^{-1}) of the global minimum from indicated sources. (I) indicates the intermolecular modes; (M) and (W) the intramolecular modes of methane and water, respectively. Frequencies of the fragment monomers are also given.

mode	*ab initio* [a]	PES-PI	PES-CSM	LMon [b]	Frag. [c]
1 (I)	49	26	47		
2 (I)	74	75	41		
3 (I)	80	86	87		
4 (I)	87	92	75		
5 (I)	111	113	113		
6 (I)	170	172	215		
7 (M)	1347	1342	1349	1342	1346
8 (M)	1349	1344	1355	1344	1346
9 (M)	1351	1353	1347	1353	1346
10 (M)	1573	1556	1559	1556	1555
11 (M)	1576	1561	1556	1563	1555
12 (W)	1651	1653	1650	1651	1649
13 (M)	3029	3027	3031	3027	3032
14 (M)	3148	3148	3156	3148	3156
15 (M)	3151	3149	3157	3149	3156
16 (M)	3159	3154	3160	3154	3156
17 (W)	3832	3829	3831	3829	3833
18 (W)	3940	3939	3941	3939	3944

[a] CCSD(T)-F12b/haTZ.
[b] Performed on PES-PI.
[c] Frequencies from the monomer PESs in Ref. 39 and 40.

weakly bound dimer. Finally, if we compare the frequencies of the intramolecular modes in the dimer with those of the isolated monomers, as a consequence of symmetry breaking, the degeneracy of the frequencies of methane split in the dimer and the magnitude of the splitting is certainly large enough to be detected experimentally. We also did the same analysis for the higher energy minimum and find that the intramolecular frequencies differ from those of the global minimum by less than 5 cm^{-1}. This is not surprising given the weak binding of the monomers and the highly delocalized nature of the ground vibrational state wave function.

The anharmonic intramolecular fundamental energies at the global minimum reference configuration with the indicated approaches are listed in Table 6, and the corresponding IR spectra are presented in Fig. 6. The spectra in Fig. 6 panel (a) and (b) are from PES-PI. The LMon frequencies and spectrum agree well with the calculation using the twelve intramolecular modes, with differences of no more than 10 cm^{-1}. The good agreement is expected, since the interaction between water and methane is weak and the normal modes of the dimer are localized in the monomer. In addition, the same LMon calculations were performed using PES-CSM and the spectrum, shown in Fig 6-(c), are in very good agreement with those from the benchmark PES-PI. Finally, there are significant shifts in the energies shown in these panels compared to

Table 6 Anharmonic intramolecular fundamental energies (cm^{-1}) of the global minimum, using the indicated method and PES. (m) and (w) indicates the intramolecular modes of methane and water

mode	12-mode/PES-PI	LMon/PES-PI	LMon/PES-CSM
7 (M)	1300	1306	1313
8 (M)	1298	1308	1319
9 (M)	1309	1315	1311
10 (M)	1521	1525	1527
11 (M)	1521	1529	1533
12 (W)	1587	1596	1595
13 (M)	2894	2894	2903
14 (M)	2993	2997	3004
15 (M)	2994	3000	3007
16 (M)	2992	3003	3008
17 (W)	3657	3653	3655
18 (W)	3741	3750	3753

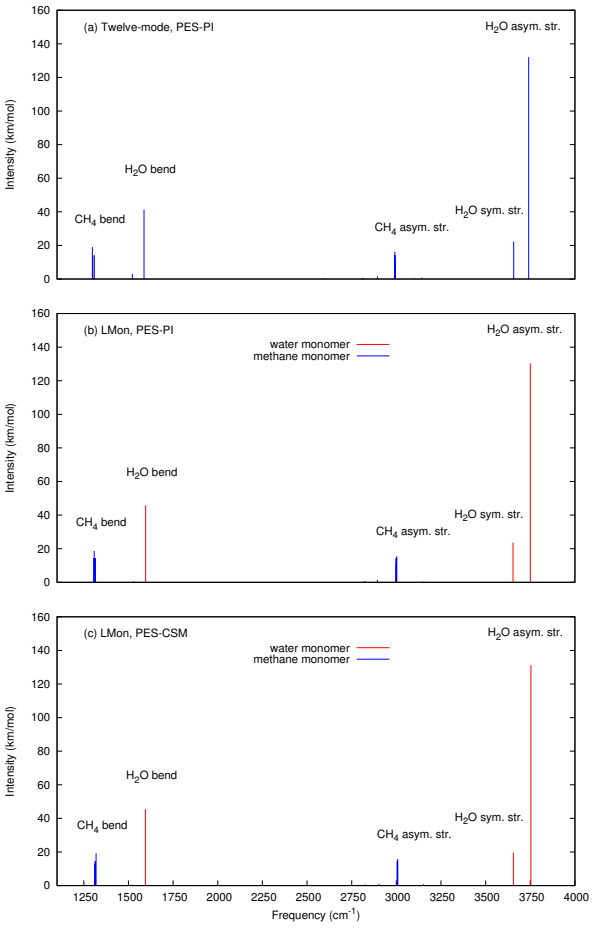

Fig. 6 IR spectra of global minimum (a) in the twelve-mode calculation using PES-PI; (b) in LMon calculation using PES-PI; (c) in LMon calculation using PES-CSM.

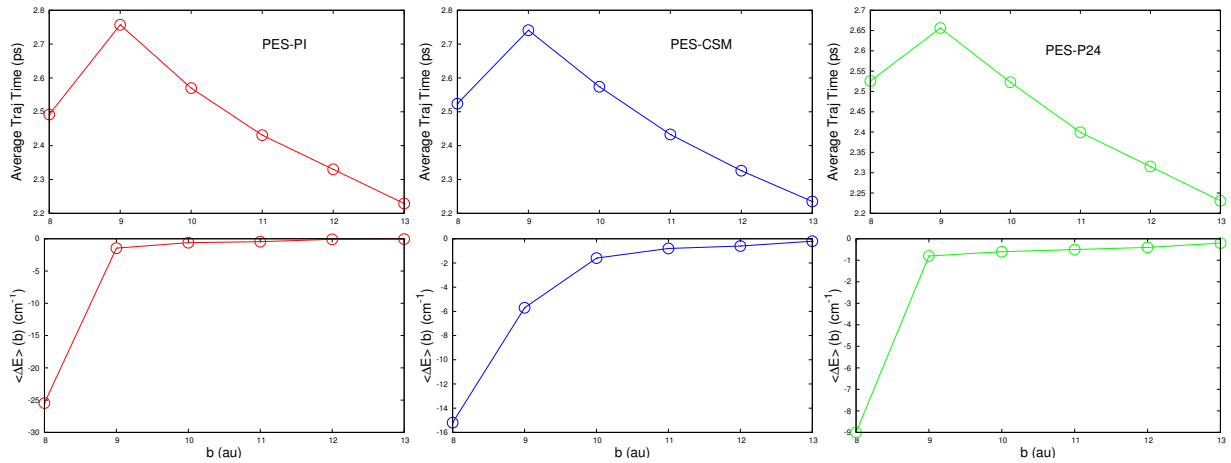

Fig. 7 Evaluation of maximum impact parameter in CH_4-H_2O scattering simulations for PES-PI, PES-CSM, and PES-P24 potentials.

the harmonic ones. The results in this figure are the ones predicted to guide experiments. We stress that these spectra are not intended to be of "line-list" quality. Clearly, such quality would require a more accurate DMS and exact ro-vibrational calculations of the transition moment.

3.3 Collisional energy transfer dynamics

In future work, we intend to investigate energy transfer collisions of methane with water using the PESs reported here. To test the suitability of these PESs for scattering calculations, we investigated the impact-parameter (b) dependence of the average trajectory time and average energy transfer, and determined the maximum impact parameter (b_{max}) in preliminary simulations of methane-water collisions. In these simulations the collisional energy was set to 1 kcal/mol. The initial internal energies were set to 10,000 cm^{-1} and 5,000 cm^{-1} for methane and water respectively. Starting internal energies were distributed by means of a microcanonical sampling. For each PES, small batches of 100 collisional trajectories were evolved for each chosen value of the impact parameter. As already pointed out in a previous work,[36] the average trajectory time is expected to peak before the b_{max} value is reached. After that, the average trajectory time drops steeply while approaching and finally exceeding b_{max}. On the other hand, the b-dependent average energy transfer ($\langle \Delta E \rangle$ (b)) is expected to approach zero at b_{max} and larger impact parameter values, since interaction and energy transfer become negligible. We identified b_{max} as the smallest impact parameter for which the two previous conditions are met, considering the condition $\langle \Delta E \rangle$ (b) ≈ 0 satisfied when $|\Delta E|$ (b) < 0.2 cm^{-1}. Fig. 7 shows that b_{max} values for PES-PI (12.5 au), PES-CSM (13.0 au), and PES-P24 (13.0 au) are in very good agreement. Furthermore, all the three average trajectory times peak at about 2.7 ps for impact parameter b=9 au. As expected, collisional energy transfer simulations are less sensitive to the potential adopted than energetics and spectroscopy calculations.

4 Summary and Conclusions

We have presented three intrinsic two-body PESs of different accuracy and complexity for the methane-water interaction energy, leading to three PESs for the methane-water dimer. The benchmark PES (PES-PI) is very accurate with an rms error of 3.5 cm^{-1}. It reproduces the *ab initio* attractive well depth and harmonic frequencies of the dimer very well. DMC calculations indicate a weak binding of the dimer, with dissociation energy of 153 ± 11 cm^{-1}, while the two monomers undergo near free internal rotation. The anharmonic vibrational frequencies and the intensity of the transitions were predicted by MULTIMODE calculations. The preliminary simulations of methane-water collisional energy transfer also show that dynamics simulations can be readily performed using our PESs.

Two other fitting procedures were considered to represent the PES. By comparing the well depth, the harmonic and anharmonic frequencies, as well as maximum impact parameter with our best PES (PES-PI), we conclude that PES-CSM is also quite accurate. The compact fitting procedure is able to speed up calculations by a factor of about ten. These results point out that the compact fit is promising for studies of more complex systems or even condensed phase clusters, where a larger number of two-body methane-water interactions necessitate to be considered. In these cases, a substantial reduction of computational times allows to follow the real dynamics of the system for much longer times. On the other hand, the sum-of-pairs potential (PES-P24) fails to identify the minimum structure of the dimer, and provides an inaccurate binding energy. However, in the preliminary and less potential-

sensitive dynamics simulations, PES-P24 provides a good estimate of the maximum impact parameter. We conclude that pairwise intrinsic two-body potentials have a restricted range of applicability, but can still be useful for dynamics simulations of very complex systems, for which too many *ab initio* energies could be required to fit a permutationally-invariant potential.

Finally, the PESs and DMS are available upon request to the authors.

Acknowledgements

This material is based upon work supported by the U.S. Department of Energy, Office of Science, Office of Basic Energy Sciences, under Award Number DE-FG02-97ER14782. C. Q. thanks NASA for financial support through Grant No. 370NNX12AF42G from the NASA Astrophysics Research and Analysis program.

References

1 E. D. Sloan and C. A. Koh, *Clathrate hydrates of natural gases*, CRC Press, Taylor & Francis Group, 3rd edn., 2008.
2 M. R. Walsh, C. A. Koh, E. D. Sloan, A. K. Sum and D. T. Wu, *Science*, 2009, **326**, 1095–1098.
3 G.-J. Guo, M. Li, Y.-G. Zhang and C.-H. Wu, *Phys. Chem. Chem. Phys.*, 2009, **11**, 10427–10437.
4 L. C. Jacobson, W. Hujo and V. Molinero, *J. Am. Chem. Soc.*, 2010, **132**, 11806–11811.
5 P. Pirzadeh and P. G. Kusalik, *J. Am. Chem. Soc.*, 2013, **135**, 7278–7287.
6 M. Lauricella, S. Meloni, N. J. English, B. Peters and G. Ciccotti, *J. Phys. Chem. C*, 2014, **118**, 22847–22857.
7 B. C. Barnes, B. C. Knott, G. T. Beckham, D. T. Wu and A. K. Sum, *J. Phys. Chem. B*, 2014, **118**, 13236–13243.
8 H. Kim, S. J. Keasler and B. Chen, *J. Phys. Chem. B*, 2014, **118**, 6875–6884.
9 C. L. Dias and H. S. Chan, *J. Phys. Chem. B*, 2014, **118**, 7488–7509.
10 G. Graziano, *J. Chem. Phys.*, 2014, **140**, 094503.
11 J. Troe and V. G. Ushakov, *J. Chem. Phys.*, 2012, **136**, 214309.
12 A. W. Jasper, J. A. Miller and S. J.Klippenstein, *J. Phys. Chem. A*, 2013, **117**, 12243–12255.
13 A. W. Jasper and J. A. Miller, *J. Phys. Chem. A*, 2009, **113**, 5612–5619.
14 A. W. Jasper and J. A. Miller, *J. Phys. Chem. A*, 2011, **115**, 6438–6455.
15 R. J. Duchovic and W. L. Hase, *J. Chem. Phys.*, 1985, **82**, 3599–3606.
16 G. Lendvay and G. C. Schatz, *J. Phys. Chem.*, 1990, **94**, 8864–8866.
17 D. C. Clary, R. G. Gilbert, V. Bernshtein and I. Oref, *Faraday Discuss.*, 1995, **102**, 423–433.
18 S. R. Ungemach and H. F. Schaefer III, *J. Am. Chem. Soc.*, 1974, **96**, 7898–7901.
19 J. J. Novoa, B. Tarron, M.-H. Whangbo and J. M. Williams, *J. Chem. Phys.*, 1991, **95**, 5179–5186.
20 G. Bolis, E. Clementi, D. H. Wertz, H. A. Scheraga and C. Tosi, *J. Am. Chem. Soc.*, 1983, **105**, 355–360.
21 D. E. Woon, P. Zeng and D. R. Beck, *J. Chem. Phys.*, 1990, **93**, 7808–7812.
22 M. M. Szczęśniak, G. Chałasiński, S. M. Cybulski and P. Cieplak, *J. Chem. Phys.*, 1993, **98**, 3078–3089.
23 M. C. Rovira, J. J. Novoa, M.-H. Whangbo and J. M. Williams, *Chem. Phys.*, 1995, **200**, 319–335.
24 Z. Cao, J. W. Tester and B. L. Trout, *J. Chem. Phys.*, 2001, **115**, 2550–2559.
25 O. Akin-Ojo and K. Szalewicz, *J. Chem. Phys.*, 2005, **123**, 134311.
26 K. L. Copeland and G. S. Tschumper, *J. Chem. Theory Comput.*, 2012, **8**, 1646–1656.
27 B. J. Braams and J. M. Bowman, *Int. Rev. Phys. Chem.*, 2009, **28**, 577–606.
28 Z. Xie and J. M. Bowman, *J. Chem. Theory Comput.*, 2010, **6**, 26–34.
29 R. Conte, P. L. Houston and J. M. Bowman, *J. Chem. Phys.*, 2014, **140**, 151101.
30 R. Conte, C. Qu, P. L. Houston and J. M. Bowman, *J. Chem. Theory Comput. to be submitted*, 2014.
31 A. J. C. Varandas and S. P. J. Rodrigues, *J. Chem. Phys.*, 1997, **106**, 9647–9658.
32 T. B. Adler, G. Knizia and H.-J. Werner, *J. Chem. Phys.*, 2007, **127**, 221106.
33 G. Knizia, T. B. Adler and H.-J. Werner, *J. Chem. Phys.*, 2009, **130**, 054104.
34 H.-J. Werner, P. J. Knowles, G. Knizia, F. R. Manby, M. Schütz, P. Celani, T. Korona, R. Lindh, A. Mitrushenkov, G. Rauhut, K. R. Shamasundar, T. B. Adler, R. D. Amos, A. Bernhardsson, A. Berning, D. L. Cooper, M. J. O. Deegan, A. J. Dobbyn, F. Eckert, E. Goll, C. Hampel, A. Hesselmann, G. Hetzer, T. Hrenar, G. Jansen, C. Köppl, Y. Liu, A. W. Lloyd, R. A. Mata, A. J. May, S. J. McNicholas, W. Meyer, M. E. Mura, A. Nicklass, D. P. O'Neill, P. Palmieri, D. Peng, K. Pflüger, R. Pitzer, M. Reiher, T. Shiozaki, H. Stoll, A. J. Stone, R. Tarroni, T. Thorsteinsson, M. Wang and A. Wolf, *MOLPRO, version 2010.1, a package of ab initio programs*, 2010, see http://www.molpro.net.
35 S. P. J. Rodrigues and A. J. C. Varandas, *J. Phys. Chem. A*, 1998, **102**, 6266–6273.
36 R. Conte, P. L. Houston and J. M. Bowman, *J. Phys. Chem. A*, 2013, **117**, 14028–14041.
37 R. Conte, P. L. Houston and J. M. Bowman, *J. Phys. Chem. A*, 2014, **118**, 7742–7757.
38 Y. Wang, X. Huang, B. C. Shepler, B. J. Braams and J. M. Bowman, *J. Chem. Phys.*, 2011, **134**, 094509.
39 R. Warmbier, R. Schneider, A. R. Sharma, B. J. Braams, J. M. Bowman and P. H. Hauschildt, *Astron. Astrophys.*, 2009, **495**, 655–661.
40 H. Partridge and D. W. Schwenke, *J. Chem. Phys.*, 1997, **106**, 4618–4639.
41 S. N. Yurchenko, J. Tennyson, R. J. Barber and W. Thiel, *J. Mol. Spectrosc.*, 2013, **291**, 69–76.
42 L. Lodi, J. Tennyson and O. L. Polyansky, *J. Chem. Phys.*, 2011, **135**, 034113.
43 J. B. Anderson, *J. Chem. Phys.*, 1975, **63**, 1499–1503.
44 J. B. Anderson, *J. Chem. Phys.*, 1976, **65**, 4121–4127.
45 A. B. McCoy, *Int. Rev. Phys. Chem.*, 2006, **25**, 77–107.
46 J. M. Bowman, S. Carter and X. Huang, *Int. Rev. Phys. Chem.*, 2003, **22**, 533–549.
47 S. Carter, H. M. Shnider and J. M. Bowman, *J. Chem. Phys.*, 1999, **110**, 8417–8423.
48 C. Qu, R. Prosmiti and J. M. Bowman, *Theor. Chem. Acc.*, 2013, **132**, 1413.
49 Y. Wang and J. M. Bowman, *J. Chem. Phys.*, 2011, **134**, 154510.
50 Y. Wang and J. M. Bowman, *J. Chem. Phys.*, 2012, **136**, 144113.
51 H. Liu, Y. Wang and J. M. Bowman, *J. Phys. Chem. Lett.*, 2012, **3**, 3671–3676.
52 H. Liu, Y. Wang and J. M. Bowman, *J. Am. Chem. Soc.*, 2014, **136**, 5888–5891.
53 J. S. Mancini and J. M. Bowman, *J. Chem. Phys.*, 2013, **139**, 164115.
54 R. Burcl, S. Carter and N. C. Handy, *Chem. Phys. Lett.*, 2003, **380**, 237–

244.
55 L. Dore, R. C. Cohen, C. A. Schmuttenmaer, K. L. Busarow, M. J. Elrod, J. G. Loeser and R. J. Saykally, *J. Chem. Phys.*, 1994, **100**, 863–876.
56 R. D. Suenram, G. T. Fraser, F. J. Lovas and Y. Kawashima, *J. Chem. Phys.*, 1994, **101**, 7230–7240.

Table of Contents

The global minimum structure of CH_4-H_2O dimer and its anharmonic vibrational spectrum from MULTIMODE calculation.